On the Extraction of Cross Sections for π^0 and η Photoproduction off Neutrons from Deuteron Data

V.E. Tarasov[1], W.J. Briscoe[2], M. Dieterle[3], B. Krusche[3], A.E. Kudryavtsev[1,2], M. Ostrick[4], I.I. Strakovsky[2]

[1] *Institute of Theoretical and Experimental Physics, Moscow, Russia*
[2] *The George Washington University, Washington, DC 20052, USA*
[3] *Department of Physics, University of Basel, Ch-4056, Basel, Switzerland*
[4] *Institut für Kernphysik, Johannes Gutenberg-Universität, Mainz, Mainz, Germany*

We discuss the procedure of extracting the photoproduction cross section for neutral pseudoscalar mesons off neutrons from deuteron data. The main statement is that the final-state interaction (FSI) corrections for the proton and neutron target are *in general* not equal, but for π^0 production there are special cases were they have to be identical and there are large regions in the parameter space of incident photon energy and pion polar angle, θ^*, where they happen to be quite similar. The corrections for both target nucleons are practically identical for π^0 production in the energy range of the $\Delta(1232)3/2^+$ resonance due to the specific isospin structure of this excitation. Also above the Δ-isobar range large differences between proton and neutron correction factors are only predicted for extreme forward angles ($\theta^* < 20^\circ$), but the results are similar for larger angles. The case of η photoproduction is also shortly considered. Numerical results for the $\gamma p \to \pi^0 p$ and $\gamma n \to \pi^0 n$ correction factors are discussed. Also the model description for the available data on the differential $\gamma d \to \pi^0 pn$ cross sections are given.

1. Introduction

We analyze the procedure of extracting π^0/η-photoproduction cross sections off neutrons and off protons from deuteron data. In both cases, this procedure takes into account the fact that the elementary γN reaction can occur on the proton as well as on the neutron of the deuteron, and that there are effects from the final-state interaction (FSI). Thus, even in quasi-free kinematics (close to the kinematics of the process on the free nucleon), there can be corrections due to this nuclear effects. In the case of photoproduction off the proton, one can compare the cross sections for free protons to that extracted from the reaction off quasi-free protons bound in the deuteron. Thus, in the proton case, there is a possibility to verify the calculation of the corrections. This verification procedure is impossible for the reaction off the neutron, since free neutron targets do not exist. The strategy for the extraction of free-neutron cross-section data from quasi-free reactions off the deuteron is then to test the FSI modelling for the proton case and apply the same

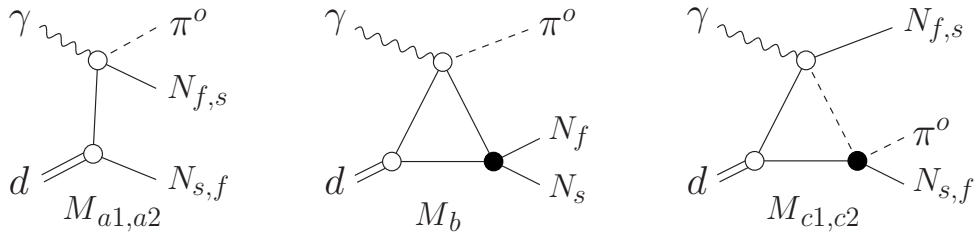

Figure 1: The impulse-approximation (M_{a1}, M_{a2}), NN-FSI (M_b) and πN-FSI (M_{c1}, M_{c2}) diagrams for the reaction $\gamma p \to \pi^0 p$. See text for definition of "fast" (N_f) and "slow" (N_s) final-state nucleons.

model to the neutron. The aim of the present note is to employ a specific approach to the FSI corrections for the deuteron data to obtain and compare the correction factors for the elementary photoproduction processes on the proton and neutron targets in wide regions of initial photon energy and of outgoing-pion angles.

2. Reaction Amplitude

Let us write down the $\gamma d \to \pi^0 pn$ amplitude (the case of η production will be discussed later on) as

$$M_{\gamma d} = M_{a1} + M_{a2} + M_b + M_{c1} + M_{c2}, \tag{1}$$

where the terms in the r.h.s. are represented in Fig. 1. The amplitude $M_{\gamma d}$ contains the impulse-approximation (IA) [1] terms M_{a1} and M_{a2} and FSI terms, where M_b is the NN-rescattering, while M_{c1} and M_{c2} are the πN-rescattering amplitudes. Hereafter, we consider the kinematics with fast and slow final state nucleons $N_f(\boldsymbol{q}_f)$ and $N_s(\boldsymbol{q}_s)$, where $\boldsymbol{q}_{f,s}$ are their momenta in the laboratory system, and $|\boldsymbol{q}_f| \gg |\boldsymbol{q}_s|$. First, let us discuss the elementary process $\gamma N \to \pi N$. In the isospin basis, the amplitude has the form [2]

$$A(\gamma N \to \pi_a N) = A_v \delta_{a3} + A_{v1} \frac{1}{2} [\tau_a, \tau_3] + A_s \tau_a \,, \tag{2}$$

where τ_a is the Pauli matrix; A_v and A_{v1} are two isovector amplitudes and A_s is the isoscalar one. For the proton and neutron targets, we have

$$A(\gamma p \to \pi^0 p) = A_v + A_s, \quad A(\gamma n \to \pi^0 n) = A_v - A_s, \tag{3}$$

i.e., in the general case, when $A_s \neq 0$, the γp and γn amplitudes are not equal. Now, we shall consider two different kinematics. Case 1 corresponds to a fast proton and a slow neutron in the final state, i.e., $N_f = p$ and $N_s = n$. We define case 2 as the result of the isospin replacement $p \leftrightarrow n$ for case 1, i.e., $N_f = n$ and $N_s = p$, with identical momenta and spins of the fast and slow nucleons. Then, the IA amplitudes M_{a1} and M_{a2} read

$$\begin{aligned} &M_{a1} = [(A_v^{(1)} + A_s^{(1)})\, \varphi_d(\boldsymbol{q}_s)], \quad M_{a2} = [(A_v^{(2)} - A_s^{(2)})\, \varphi_d(\boldsymbol{q}_f)] \quad \text{(case 1)}; \\ &M_{a1} = [(A_v^{(1)} - A_s^{(1)})\, \varphi_d(\boldsymbol{q}_s)], \quad M_{a2} = [(A_v^{(2)} + A_s^{(2)})\, \varphi_d(\boldsymbol{q}_f)] \quad \text{(case 2)}. \end{aligned} \tag{4}$$

where $\varphi(\boldsymbol{q})$ is the deuteron wave function (DWF). Hereafter in this paper, we consider only the isospin structure of the amplitudes and use the short notation $[\cdots]$, which means that all particle momenta and spins are properly taken into account. More detailed expressions with all the variables written out can be found, e.g., in Refs. [3–5] (see also references therein). The superscripts "(1)" and "(2)" of the terms $A^{(1)}_{v,s}$ and $A^{(2)}_{v,s}$ mean that they are taken at different values of spin and momentum variables due to the replacement $N_f \leftrightarrow N_s$, i.e., $A^{(1)}_{v,s} \not\equiv A^{(2)}_{v,s}$. Both amplitudes M_{a1} and M_{a2} change from case 1 to case 2 because the relative sign of the term A_s changes. Since $|\boldsymbol{q}_s| \ll |\boldsymbol{q}_f|$, we have $\varphi(\boldsymbol{q}_s) \gg \varphi(\boldsymbol{q}_f)$ and $|M_{a1}| \gg |M_{a2}|$. Thus, the leading diagram is M_{a1}, i.e., the reaction $\gamma d \to \pi^0 pn$ proceeds mainly through the subprocess $\gamma p \to \pi^0 p$ or $\gamma n \to \pi^0 n$ in case 1 or 2, respectively (the detectable recoil nucleon is the participant of the reaction).

Now consider the NN-FSI diagram M_b in Fig. 1. First, let us introduce the NN-scattering amplitude in the form

$$M(N_1N_2 \to N_3N_4) = \frac{1}{2}M_0(\chi_3^+\chi_4^c)(\chi_2^{c+}\chi_1) + \frac{1}{2}M_1(\chi_3^+\boldsymbol{\tau}\chi_4^c)(\chi_2^{c+}\boldsymbol{\tau}\chi_1). \tag{5}$$

Here: χ_{1-4} are the nucleon isospinors; $\chi^c \equiv \tau_2\chi^*$, $\boldsymbol{\tau} = (\tau_1, \tau_2, \tau_3)$, where τ_{1-3} are the isospin matrices; M_0 and M_1 are the isoscalar and isovector NN amplitudes. Making use of Eqs. (2) and (5), after calculation with isospin variables one obtains the NN-FSI amplitude M_b in the form

$$\begin{aligned} M_b &= \textstyle\int [A_v M_0 + A_s M_1] \quad \text{(case 1)}, \\ M_b &= \textstyle\int [A_v M_0 - A_s M_1] \quad \text{(case 2)}, \end{aligned} \tag{6}$$

where $\int [\cdots]$ denotes the integration over the intermediate momentum (and sum over intermediate spin states) in the triangle diagram M_b in Fig. 1. Eqs. (6) show that the isovector and isoscalar γN amplitudes A_v and A_s couple with I=0 and I=1 pn amplitudes M_0 and M_1, respectively. This follows from the simple consideration that for the final $\pi^0(pn)$ system with total I= 0 (1) the pn system should be in an I = 1 (0) state. From Eq. (5), one can get "elastic" and "charge-exchange" pn amplitudes as

$$M^{el}_{pn} = M(pn \to pn) = \frac{1}{2}(M_1 + M_0), \qquad M^{cex}_{pn} = M(np \to pn) = \frac{1}{2}(M_1 - M_0), \tag{7}$$

and rewrite Eq. (6) in the more illustrative form

$$\begin{aligned} M_b &= \textstyle\int [(A_v + A_s)M^{el}_{pn} - (A_v - A_s)M^{cex}_{pn}] \quad \text{(case 1)}, \\ M_b &= \textstyle\int [(A_v - A_s)M^{el}_{pn} - (A_v + A_s)M^{cex}_{pn}] \quad \text{(case 2)}. \end{aligned} \tag{8}$$

The amplitude M_b is represented by two terms. In case 1, the first (second) term contains the photoproduction amplitude $\gamma p \to \pi^0 p$ ($\gamma n \to \pi^0 n$) and subsequent rescattering of the fast proton (neutron) on the slow neutron (proton). Thus, the first term contains the elastic pn amplitude M^{el}_{pn} (fast proton $\to$ fast proton), while the second – charge-exchange one M^{cex}_{pn} involves the fast neutron $\to$ fast proton scattering. The changes for case 2 are obvious. In both cases, the relative sign "$-$" between two terms in Eq. (8) arises from

the isospin antisymmetry of the DWF with respect to the nucleons. In both Eqs. (6) and (8), we again follow only the isospin structure of the amplitude and show that the only difference between the results comes from the different relative sign of the term A_s in cases 1 and 2. Considering the πN-FSI diagrams M_{c1} and M_{c2} in Fig. 1, we also obtain for the general case that both these amplitudes change from case 1 to case 2 due to the different sign of the terms, containing the isoscalar $\gamma N \to \pi N$ amplitude A_s. Hereafter in the present paper, we neglect the πN-FSI amplitudes, since their role was found to be small in Refs. [4–6], and negligible at energies E above 200 MeV [5]. Then the total $\gamma d \to \pi^0 pn$ amplitude $M_{\gamma d}$ can be expressed in the form

$$M_{\gamma d} = M_{a1} + \Delta, \quad \Delta = M_{a2} + M_b, \tag{9}$$

where the IA amplitude M_{a1} is the leading-order term (quasi-free production), and Δ includes the suppressed IA diagram M_{a2} and the NN-FSI diagram M_b. In quasi-free kinematics with fast and slow final-state nucleons, Δ is a relatively small correction term in comparison to the main one M_{a1}. In this kinematics the relative momentum between the two final-state nucleons is large, and the contribution from NN-FSI is suppressed, i.e., the Migdal-Watson effect [7] from s-wave NN-FSI at small relative momenta is suppressed. The quasi-free kinematics also implies not very small momentum transfer from the initial photon to the final pion, and thus, the FSI effect doesn't essentially cancell the IA amplitudes due to the orthogonality of the final pn state to the wave function of the initial deuteron. We shall return to this point below in Sects. **4** and **5**.

3. Extraction Procedure for $\gamma N \to \pi^0 N$ Reactions

We now discuss the procedure of extracting the γN-reaction cross section from the deuteron data. First, consider case 1 (fast final-state proton, slow neutron). In quasi-free kinematics one has the relation [8] (more details are given in the Appendix)

$$\frac{d\sigma}{d\Omega}(\gamma p \to \pi^0 p) = \frac{1}{n(\boldsymbol{q}_s)} \frac{d\sigma(\gamma d)}{d\Omega\, d\boldsymbol{q}_s}, \quad n(\boldsymbol{q}_s) = \frac{E'_\gamma}{E_\gamma}\, \rho(|\boldsymbol{q}_s|). \tag{10}$$

Here: $d\Omega$ is the solid angle element of the outgoing π^0 in the $\pi^0 p_f$ center-of-mass frame with the z-axis directed along the photon beam; E_γ and E'_γ are the photon laboratory energies in the γd process and the $\gamma p \to \pi^0 p$ subprocess, and $E'_\gamma/E_\gamma = 1 + (|\boldsymbol{q}_s|/E_s)\cos\theta_s$, where E_s and $\cos\theta_s$ are the total energy and polar angle (z-axis along the photon beam) of the final slow neutron n_s in the laboratory system. The momentum distribution in the deuteron is given by $\rho(q) = (2\pi)^{-3}[u^2(q) + w^2(q)]$ ($q = |\boldsymbol{q}|$) where $u(q)$ and $w(q)$ are the S- and D-wave parts of the DWF. It is normalized to $\int \rho(q)\, d\boldsymbol{q} = 1$. One can improve Eq. (10), taking FSI corrections into account. With these corrections, we have

$$\frac{d\sigma}{d\Omega}(\gamma p \to \pi^0 p) = \frac{R_p}{n(\boldsymbol{q}_s)} \frac{d\sigma(\gamma d)}{d\Omega\, d\boldsymbol{q}_s}. \tag{11}$$

The extraction procedure for the $\gamma p \to \pi^0 p$ reaction implies Eq. (11) to be utilized with the deuteron cross section $d\sigma(\gamma d)/d\Omega\, d\boldsymbol{q}_s$, taken from the data. Here, the correction factor

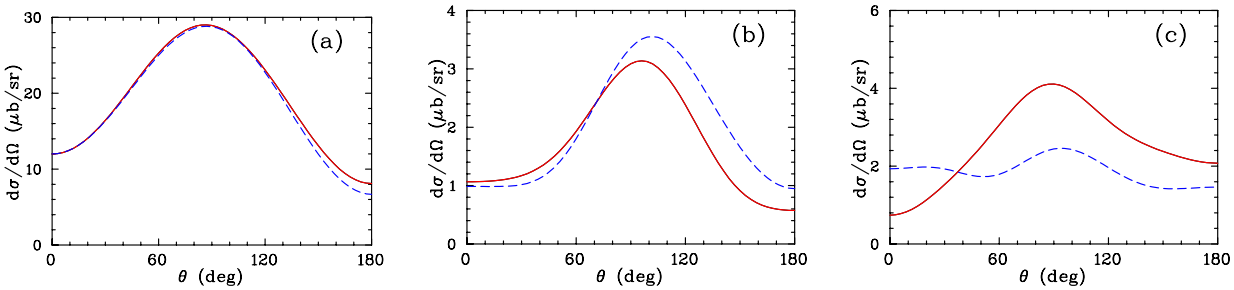

Figure 2: (Color online) The differential cross sections of the $\gamma p \to \pi^0 p$ (red solid curves) and $\gamma n \to \pi^0 n$ (blue dashed curves) reactions at several photon energies $E_\gamma = 340$ (a), 630 (b) and 787 MeV (c), which correspond to $\Delta(1232)3/2^+$, $N(1440)1/2^+$, and $N(1535)1/2^-$ regions, respectively.

R_p can be obtained from the model as

$$R_p = \frac{d\sigma^{(p)}(\gamma d)}{d\Omega\, d\boldsymbol{q}_s} \Big/ \frac{d\sigma(\gamma d)}{d\Omega\, d\boldsymbol{q}_s}, \tag{12}$$

where the cross sections $d\sigma^{(p)}(\gamma d)$ is calculated from the main IA diagram M_{a1}, while $d\sigma(\gamma d)$ is obtained from the full amplitude $M_{\gamma d} = M_{a1} + \Delta$ in Eqs. (9) and should restore the experimental data. Consider now case 2 (fast neutron, slow proton). Instead of Eqs. (11) and (12), we obtain

$$\frac{d\sigma}{d\Omega}(\gamma n \to \pi^0 n) = \frac{R_n}{n(\boldsymbol{q}_s)} \frac{d\sigma(\gamma d)}{d\Omega\, d\boldsymbol{q}_s}, \qquad R_n = \frac{d\sigma^{(n)}(\gamma d)}{d\Omega\, d\boldsymbol{q}_s} \Big/ \frac{d\sigma(\gamma d)}{d\Omega\, d\boldsymbol{q}_s}, \tag{13}$$

where $d\Omega$ is the solid angle element of the outgoing π^0 in the $\pi^0 n_f$ center-of-mass frame with the z-axis directed along the photon beam. All other notations are the same as in Eqs. (11) and (12) with the replacements $p_f \to n_f$ and $n_s \to p_s$. Here, the cross section $d\sigma^{(n)}(\gamma d)$ is also calculated with the main diagram M_{a1}, but the fast nucleon is a neutron. The correction factors R_p in Eq. (12) (case 1) and R_n in Eqs. (13) (case 2) are calculated through the amplitudes given by Eqs. (4) and (6). Going from case 1 to case 2, we change only the relative sign of the isoscalar photoproduction amplitude A_s in these Eqs. Thus, in the general case

$$R_n \neq R_p. \tag{14}$$

However, when $A_s = 0$ or $A_v = 0$ in Eq. (2), we get $R_n = R_p$. In this particular cases, the differential cross sections of the $\gamma p \to \pi^0 p$ and $\gamma n \to \pi^0 n$ reactions are equal.

3.1 Comment on the $\Delta(1232)3/2^+$ Region

Consider the π^0 photoproduction in the $\Delta(1232)3/2^+$ region. Supposing that in this region ($E_\gamma \approx 340$ MeV) the $\gamma N \to \pi^0 N$ proceeds through $\Delta(1232)3/2^+$, we obtain $A_s = 0$ due to isospin conservation. In this case, we get $R_n = R_p$, i.e., the correction factors for the reactions $\gamma p \to \pi^0 p$ and $\gamma n \to \pi^0 n$ appear to be the same, and we should also have

equal differential cross sections for these reactions. To illustrate this, we reconstruct in Fig. 2 these cross sections at several energies, obtained with the $\gamma N \to \pi N$ amplitude taken from the SAID database [9]. Fig. 2 shows that proton and neutron cross sections are very close to each other in the $\Delta(1232)3/2^+$ region ($E_\gamma = 340$ MeV). At higher energies, the contributions from $N(1440)1/2^+$ and $N(1535)1/2^-$ become important, the isoscalar amplitude $A_s \neq 0$, and the difference between proton and neutron differential cross sections is visible. The main (M_{a1}) and FSI-correction (Δ) terms in the $\gamma d \to \pi^0 pn$ amplitude $M_{\gamma d}$ (9) also become different in cases 1 and 2, and we get Ineq. (14).

3.2 Comment on the η-Photoproduction Case

Let us comment on the case of η photoproduction on the nucleon ($\gamma N \to \eta N$) and deuteron ($\gamma d \to \eta pn$). The amplitude on the nucleon has isospin structure $A(\gamma N \to \eta N) = A_v \tau_3 + A_s$, which gives

$$A(\gamma p \to \eta p) = A_v + A_s, \qquad A(\gamma n \to \eta n) = -A_v + A_s, \tag{15}$$

The difference with the π^0 case is that the isovector amplitude A_v changes sign for η production. Thus, the amplitudes M_{a1}, M_{a2}, and M_b on the deuteron with the π^0 replaced by an η are given by the same Eqs. (4), (6) and (8) with small modifications, i.e., the amplitude A_v (instead of A_s) changes sign when going from case 1 (fast proton) to case 2 (fast neutron). Thus, we arrive at the same conclusion (Eq. 14) in the general case of $A_v \neq 0$ and $A_s \neq 0$. Addition of ηN-FSI amplitudes, similar to M_{c1} and M_{c2} in Fig. 1, or the $\gamma d \to \eta pn$ amplitude with intermediate pion photoproduction followed by the $\pi N \to \eta N$ subprocess also lead in general to $R_p \neq R_n$. However, one should note that in this case FSI effects seem to be much smaller than for π^0 photoproduction. The experimental data [14, 15] show that $R_p \approx 1$ over a wide range of incident photon energies and η c.m. polar angles. A major difference to π^0 photoproduction is that this reaction is dominated for not too high incident photon energies by the excitation of S_{11} resonances via the E_{0^+} spin-flip multipole. This means that in quasi-free production off the deuteron, the final state nucleons are dominantly in a spin-singlet, while for π^0 production the spin-triplet configuration of the deuteron dominates the final state. This effect (different spin configuration) of initial (deuteron) and final np-system suppresses the role of FSI in the η case in comparison with the π^0-production case. The incoherent η-photoproduction off the deuteron was studied in a number of papers (see Ref. [16] and references therein), and the FSI effects were found to be important only in the very nearthreshold region. At higher energies, they are quite small [16], except for special kinematic configurations, where the IA contributions are suppressed. Theoretical results of Ref. [16] show visible sensitivity of some polarization observables to ηN and intermediate-pion ($\pi N \to \eta N$) FSI effects, but this issue is beyond the scope of the present paper.

4. Numerical Results

Here, we perform some numerical comparison of the correction factors R_p (12) and R_n (13) to illustrate Ineq. (14). Let us briefly describe the ingredients used in the calculation of the reaction amplitude $M_{\gamma d}$ (1). We use the elementary $\gamma N \to \pi N$ amplitudes,

generated through the GW pion photoproduction multipoles [10]. For the NN-FSI term M_b in Fig. 1, we include the s-wave pn-scattering amplitudes M_0 and M_1, introduced in Eq. (5). These invariant amplitudes for $N_1N_2 \to N_3N_4$ read

$$M_0 = 8\pi\sqrt{s}\, f_{pn}^{(0)}(p)(\varphi_3^+ \boldsymbol{\sigma} \varphi_4^c)(\varphi_2^{c+} \boldsymbol{\sigma} \varphi_1), \quad M_1 = 8\pi\sqrt{s}\, f_{pn}^{(1)}(p)(\varphi_3^+ \varphi_4^c)(\varphi_2^{c+} \varphi_1) \qquad (16)$$

($\sqrt{s}$ is the effective NN-system mass). Here: $\varphi_{1,2,3,4}$ are the nucleon Pauli spinors ($\varphi^+\varphi = 1$); $\varphi^c = \sigma_2\varphi^*$. The amplitude $M_0(M_1)$ with isospin $I=0(1)$ corresponds to the total spin $S = 1(0)$. The amplitudes $f_{pn}^{(0,1)}(p)$, where $p = |\boldsymbol{p}|$ is the relative momentum in the NN system, are expressed through the scattering lengths $a_{0,1}$ and effective radii $r_{0,1}$, i.e.,

$$f_{pn}^{(0,1)}(p) = \frac{1}{-a_{0,1}^{-1} + \frac{1}{2} r_{0,1} p^2 - ip}, \qquad f_{pn}^{(0,1)\,off}(q,p) = \frac{p^2 + \beta_{0,1}^2}{q^2 + \beta_{0,1}^2} f_{pn}^{(0,1)}(p), \qquad (17)$$

where $f_{pn}^{(0,1)\,off}(q,p)$ are the off-shell NN-amplitudes, and $q = |\boldsymbol{q}|$ is the relative momentum of the intermediate nucleons. The off-shell dependence of $f_{pn}^{(0,1)\,off}(q,p)$ is introduced through the monopole-type formfactor, as given in Eq. (17), with parameters $\beta_{0,1}$. We take the typical value $\beta_{0,1} = 1.2$ fm^{-1} (the same as in Refs. [3, 5]). For $a_{0,1}$ and $r_{0,1}$, we use the known values [11]: $a_0 = 5.4$ fm, $r_0 = 1.7$ fm, $a_1 = -24$ fm, and $r_1 = 2.7$ fm. Hereafter in the present paper, we neglect higher partial waves ($L > 0$) in the NN-scattering amplitude. To simplify the calculation of the NN-FSI term M_b [Fig. 1], we also take the amplitude of the $\gamma N \to \pi^0 N$ subprocess out of the loop integral over the intermediate momentum in this term. This approximation allows us to calculate analytically the FSI term M_b. The more precise calculations with higher NN partial waves included are planned for the future publication. The DWF was taken from the Bonn potential (full model) [13].

The results of the model for differential cross sections $d\sigma/d\Omega^*$ of the reaction $\gamma d \to \pi^0 pn$ for several photon laboratory energies E are compared in Fig. 3 to experimental data from Ref. [17] [plots (a-f)] and to recent data from Ref. [18] [plots (g-m)]. Here, θ^* is the polar angle of the outgoing π^0 in the c.m. system of the incident photon and a nucleon at rest with z-axis directed along the photon momentum. The dotted curves show the contributions from the IA term $M_a = M_{a1} + M_{a2}$, while the dashed ones represent the results obtained with the full amplitude $M_{\gamma d} = M_{a1} + M_{a2} + M_b$ (9). Comparison of these curves shows an important role of the NN-FSI, which essentially decrease the cross sections at low energies in line with other papers [4–6]. At higher energies [plots(j-m)], the FSI effect is very small, except the region of small angles θ^*, where the effect is sizeable. Our model predictions (dashed curves) sizeably overestimate the data, but the shape of the differential cross sections in the main is reproduced. It is quite possible that the full account of multiple-scattering diagrams (not only M_b term in Fig. 1) may lead to destructive interference and decrease the cross sections, insignificantly affecting the shape of the distributions.

Let us try to improve the theoretical description, taking into account that the $\gamma N \to \pi N$ amplitudes in the diagrams M_{a1}, M_{a2} and M_b [Fig. 1] are not on the mass shell. Let us multiply the elementary $\gamma N \to \pi N$ amplitude by the off-shell correction factor of the form

$$F(q_\gamma, q'_\gamma) = \frac{\Lambda^2 + q_\gamma^2}{\Lambda^2 + q_\gamma'^2}, \qquad (18)$$

where q_γ (q'_γ) is the photon c.m. momentum in the $\gamma N \to \pi N$ reaction, calculated with on-shell (off-shell) initial nucleon at a given effective γN mass. We add this factor to the IA amplitudes M_{a1} and M_{a2}. For simplicity, we neglect this correction in the NN-FSI term, where the momenta of the nucleons in the deuteron vertex are effectively small in the loop integral, and the off-shell effect is expected to be small. On the other hand, we expect that the IA contributions at high energies [Fig, 3, plots (j-m), dotted curves], where FSI effects are very small, are overestimated in the model and should be suppressed. Solid curves in Fig. 3 show the off-shell corrected results from the full amplitude $M_{\gamma d}$ (9) with $\Lambda = 1$ fm^{-1} in Eq. (18) (we use the value of the same order of magnitude as $\beta' s$ in Eqs. (17)). The role of the off-shell correction is negligible at low energies [Fig. 3, plots (a-c)], but visibly decreases the cross sections at higher energies, and the theoretical description looks better. However, the model still overestimates the data, and varying the value of Λ (18), one can not decrease the predicted cross sections in accordance with the data. Here we finish the comparison of the model with the data, leaving further developments, which perhaps should involve the multiple-scattering diagrams, to the next publications.

Now consider the theoretical predictions for the correction factors R_p and R_n, introduced in Sect. 3. They are given in Fig. 4 at the same photon energies as in Fig. 2. For illustrative purposes the results are "averaged" over the spectator momentum $\boldsymbol{q}_s$, where $R_{p,n}$ are defined as

$$R_p = \frac{d\sigma^{(p)}(\gamma d)}{d\Omega} \Big/ \frac{d\sigma(\gamma d)}{d\Omega}, \qquad R_n = \frac{d\sigma^{(n)}(\gamma d)}{d\Omega} \Big/ \frac{d\sigma(\gamma d)}{d\Omega}, \tag{19}$$

where the differential cross sections are integrated over the kinematic region $|\boldsymbol{q}_f| > |\boldsymbol{q}_s|$. Hereafter, we do not apply the off-shell correction Eq. (18) to the $\gamma N \to \pi N$ amplitude. The plots at the top [(a-c)] show the factor R_p (19) for case 1 with fast protons and slow neutrons, while the plots at bottom [(d-f)] show the factor R_n for case 2 with fast neutrons and slow protons. The polar angle θ^* of the outgoing pion is defined in the $\pi^0 p$ (case 1) or $\pi^0 n$ (case 2) c.m. frame. The types of curves in Fig. 4 specify the calculation of the cross sections $d\sigma(\gamma d)/d\Omega$, i.e., the denominators in Eqs. (19). The dashed curves are the results obtained with the full IA amplitude $M_{a1} + M_{a2}$ for these cross sections, i.e., they include the correction for the "suppressed" IA term M_{a2}. Addition of the NN-FSI term M_b leads to the solid curves. We see that the "suppressed" IA term M_{a2} alone already produces a sizeable deviation $R_{p,n} \neq 1$, which increases to small angles. The NN-FSI term M_b, when included, considerably affects the results. Both terms (M_{a2} and M_b) essentially affect the results at small angles θ^* (pions emitted at forward angles), where the configuration with small relative momenta between the final-state nucleons dominates, and this θ^* region narrows with the increasing photon energy. At higher angles, both effects are negligible, and $R_{p,n} \approx 1$. At $E_\gamma = 340$ MeV [plots (a, d)], we obtain a large effect at $\theta^* \sim 0$, where $R_{p,n} \sim 6$. We qualitatively interpret this results as a self-cancellation effect in the full amplitude $M_{\gamma d} = M_{a1} + M_{a2} + M_b$ due to the non-ortogonality between the initial deuteron state and the final NN plane-wave state. This cancellation should enhance at small momentum transfers Δ from the initial photon to the final pion, decreasing the denominators $d\sigma(\gamma d)/d\Omega$ in Eqs. (19). The effective value of Δ is minimal at $\theta^* = 0$

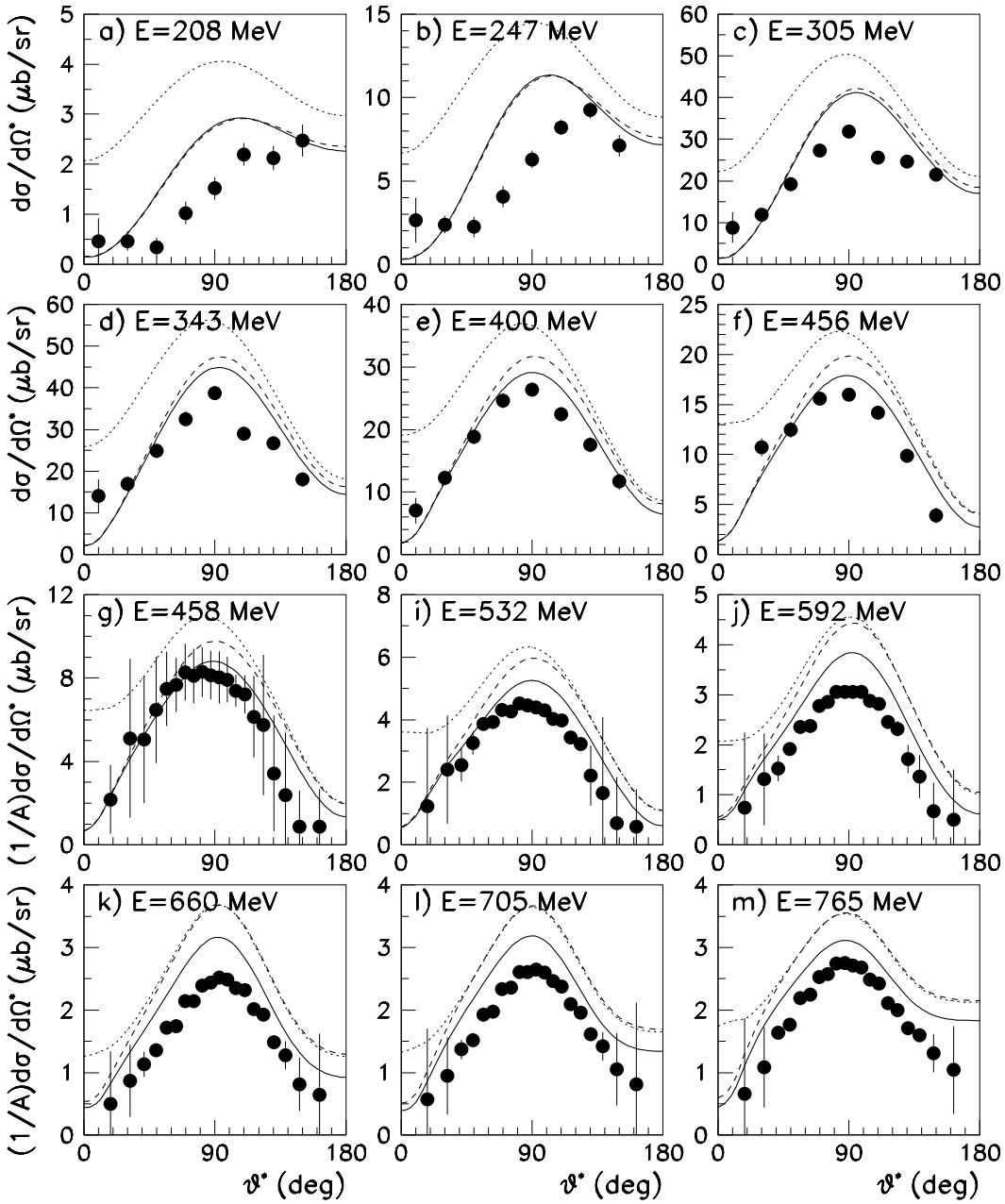

Figure 3: The differential cross sections of the $\gamma d \to \pi^0 pn$ for several values of the photon-beam laboratory energy E vs. θ^* (the angle θ^* is defined in the text). The curves show the contributions: dotted – from the IA amplitudes $M_{a1,a2}$ [Fig. 1]; dashed – from the total amplitude $M_{\gamma d}$ (9) with the NN-FSI. Solid curves include also the off-shell correction (18) for the $\gamma N \to \pi N$ amplitude. The filled circles: in the plots (a-f) – the data from Ref. [17] (error bars include statistical uncertainties only); in the plots (g-m) – the data from Ref. [18] (error bars include statistical and systematic uncertainties in quadratures), multiplied by $1/A$ ($A = 2$ for the deuteron).

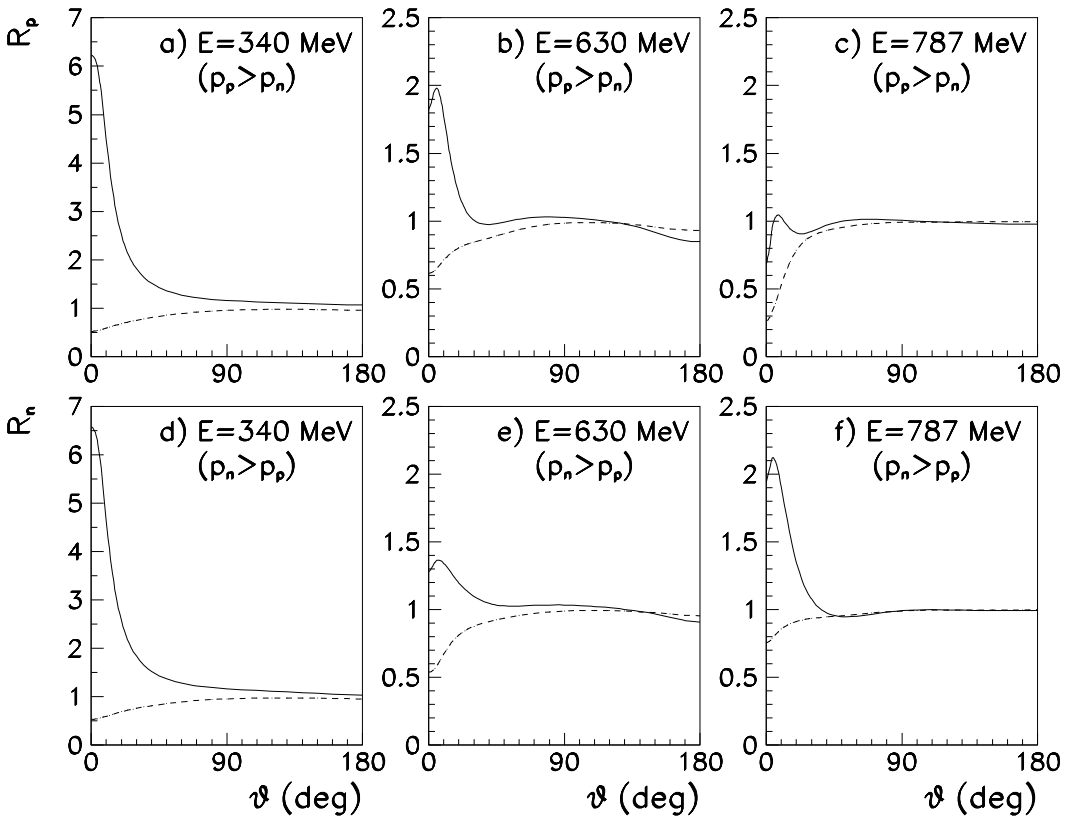

Figure 4: The correction factors R_p [plots (a-c)] and R_n [plots (d-f)], calculated according to Eqs. (19) from the reactions $\gamma_d \to \pi^0 p_f n_s$ and $\gamma d \to \pi^0 n_f p_s$, respectively. Left, middle and right plots – the results for $E_\gamma = 340$, 630, and 787 MeV, respectively. The numerators $d\sigma^{(p,n)}/d\Omega$ in Eq. (19) are obtained from the leading IA amplitude M_{a1}. Successive addition of the "suppressed" IA term M_{a2} and NN-FSI term M_b, when calculating the denominators $d\sigma/d\Omega$ in Eqs. (19), leads to dashed and solid curves, respectively.

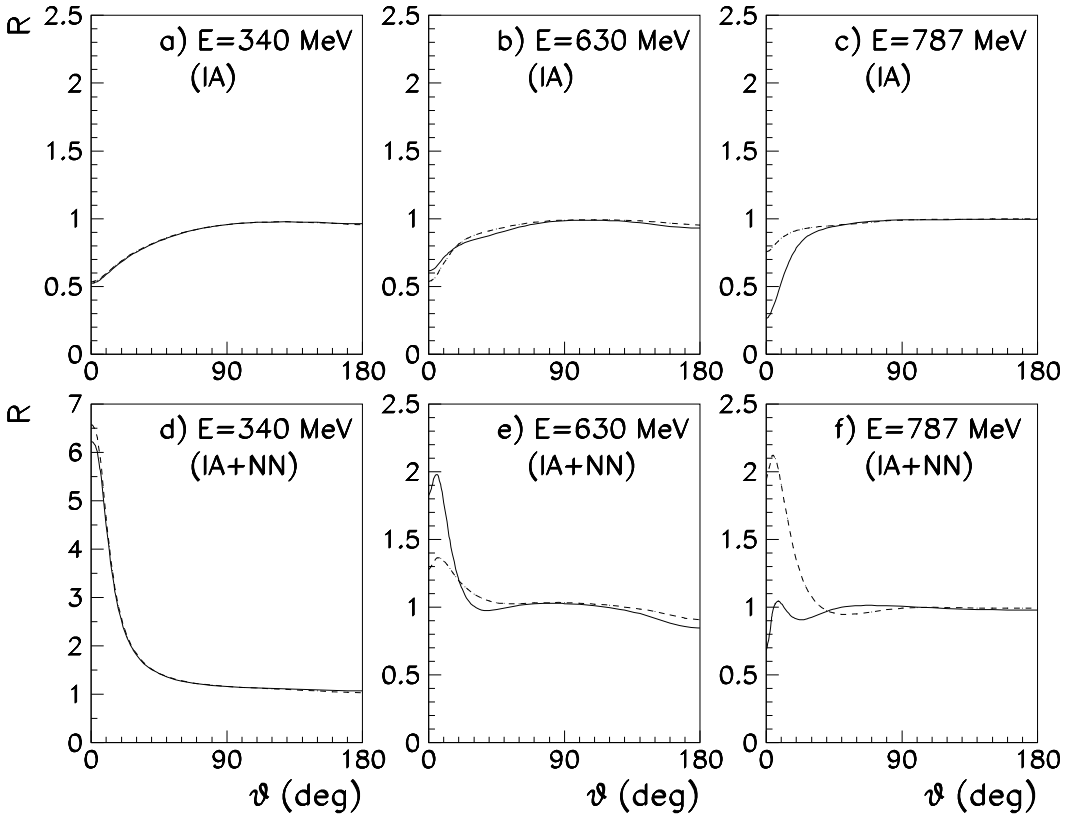

Figure 5: Comparison of the correction factors R_p (solid curves) and R_n (dashed curves) at the same energies E as in Fig. 4. Upper [(*a*-*c*)] and lower [(*d*-*f*)] plots correspond to the variants shown by dashed and solid curves in Fig. 4, respectively (see notations therein).

and decreases with the increasing photon energy. We shall also mark this point in the Conclusion.

The same results are shown in Fig. 5 as a comparison of R_p (solid) and R_n (dashed) factors. The top [(*a*-*c*)] and and bottom [(*d*-*f*)] rows show these factors for successive inclusion of the "suppressed" IA term M_{a2} and NN-FSI term M_b for the denominators $d\sigma(\gamma d)/d\Omega$ in Eqs. (19). At $E_\gamma = 340$ MeV, i.e., in the $\Delta(1232)3/2^+$ region, we have $R_p = R_n$ to a good accuracy, since the role of the isoscalar $\gamma N \to \pi N$ amplitude A_s is negligible. At higher energies (630 and 787 MeV), we observe that $R_p \neq R_n$, because both isovector and isoscalar amplitudes (A_v and A_s) contribute. This difference is considerable at small angles θ^* where the role of the "suppressed" IA term M_{a2} and NN-FSI is enhanced. Thus, the results in Fig. 5 illustrate our analytical considerations discussed above, which lead to the general in Ineq. (14).

5. Conclusion

We see that the values $R_{p,n}$ strongly differ from 1 at small angles θ^*. One obtains the large values $R_{p,n}$ when including the NN-FSI diagram, which decreases the differential cross sections at small angles. It means that at small momentum transfers the FSI term essentially cancels the IA terms due to orthogonality of the final pn-state to the deuteron wave function. This cancellation suppresses the denominators in Eqs. (12) and (13), i.e., the cross sections on the deuteron, and leads to the growth of $R_{p,n}$. We plan to return to this point with more details in the next papers. This effect, not connected with the Migdal-Watson effect [7], was considered earlier in Ref. [19] (see also Ref. [4]). Concerning the physical meaning of the results one should remember that the photon has no definite isospin. For any given process, it may be represented as a superposition of I = 0 and I = 1 states, i.e., $|\gamma\rangle = c_0|0\rangle + c_1|1\rangle$, where the coefficients $c_{0,1}$ depend on the reaction amplitude. Let us apply the charge symmetry (CS) operator [20], which is the rotation by 180° about the y-axis in isospin space with the z-axis related to the charge, to the process $\gamma d \to \pi^0 p_f n_s$. We denote fast and slow protons (neutrons) as $p_{f,s}$ ($n_{f,s}$). The CS rotation of the initial and final particles gives

$$\begin{aligned} &|\gamma\rangle \to |\gamma'\rangle = c_0|0\rangle - c_1|1\rangle \neq |\gamma\rangle, \quad |d\rangle \to |d\rangle, \quad |\pi^0\rangle \to -|\pi^0\rangle, \\ &|p\rangle \to |n\rangle, \quad |n\rangle \to -|p\rangle, \quad |pn\rangle_I \to \pm\,|pn\rangle_I \;\; (+,- \text{ for } I = 0,1). \end{aligned} \tag{20}$$

Then for the amplitudes of interest, we obtain

$$M(\gamma d \to \pi^0 p_f n_s) = M(\gamma' d \to \pi^0 n_f p_s) \neq M(\gamma d \to \pi^0 n_f p_s). \tag{21}$$

Here the first equality is the result of the CS rotation. The second inequality means that the corresponding amplitudes are different because the initial photons are different, i.e., $|\gamma\rangle \neq |\gamma'\rangle$. As a result, we obtain $M(\gamma d \to \pi^0 p_f n_s) \neq M(\gamma d \to \pi^0 n_f p_s)$, and that is the general reason for the Eq. (14). In the $\Delta(1232)3/2^+$ range, where the isoscalar $\gamma N \to \pi N$ amplitude A_s is negligibly small, the proton and neutron correction factors are equal, $R_p = R_n$, to a good accuracy. This means that in this region one can extract the $\gamma n \to \pi^0 n$ differential cross section from the $\gamma d \to \pi^0 n_f p_s$ data by making use of the proton

factor R_p. This is convenient, since R_p can be directly obtained from Eq. (11), making use of the data on the free proton ($\gamma p \to \pi^0 p$) and on the deuteron ($\gamma d \to \pi^0 p_f n_s$). In this way one can also verify the model predictions for R_p obtained from Eq. (12). In the region above the $\Delta(1232)3/2^+$, where both isovector and isoscalar $\gamma N \to \pi N$ amplitudes are important, we have Ineq. (14). The main R_p/R_n differences in our results are observed at small angles θ^*, where contributions of the "suppressed" IA amplitude M_{a2} or NN-FSI terms are important. However, there is a wide range of large angles θ^*, where we have approximately $R_p = R_n$. To the end of this paper it is worth saying that the results of calculations, presented in Figs. 3−5, were obtained not with the full program, but include a number of approximations with only s-wave NN-rescatterings taken into account and simplified version of the loop integral in the FSI term M_b as was mentioned in Sect. **4**. We leave more precise full calculations for the future publication.

Acknowledgements

The authors are thankful to V. V. Kulikov for useful discussion. This material is based upon work supported by the U.S. Department of Energy, Office of Science, Office of Nuclear Physics, under Award Number DE-FG02-99-ER41110 and the DFG under Grant No. SFB 1044. M. D. and B. K. acknowledge support from Schweizerischer Nationalfonds. A. E. K. thanks Grant No. NS.3172.2012.2 for partial support. V. E. T. and A. E. K. thank the Institute for Kernphysik at Mainz where part of this work was performed for hospitality and support.

Appendix:

On the Relation between the Cross Sections on the Nucleon and Deuteron

In quasi-free kinematics, the reaction $\gamma d \to \pi^0 p_f n_s$ goes predominantly via the diagram M_{a1} in Fig. 1. For definiteness, we consider case 1 with a fast proton and a slow neutron. In this approximation, the differential cross section on the deuteron is related to that on the proton ($\gamma p \to \pi^0 p$) through Eq. (10), which is well-known [8]. Here, we give some explanations, which may be useful when analysing experimental data. Hereafter, we use the notations

$$k_\gamma = (E_\gamma, \boldsymbol{q}_\gamma), \quad k_d = (m_d, \vec{0}), \quad k_\pi = (E_\pi, \boldsymbol{q}_\pi), \quad k_f = (E_f, \boldsymbol{q}_f), \quad k_s = (E_s, \boldsymbol{q}_s) \qquad \text{(A.1)}$$

for the 4-momenta of the photon, deuteron, pion, fast proton and slow neutron (spectator), respectively. The total energies and 3-momenta in the laboratory frame (deuteron rest frame with z-axis along the photon beam) are given in brackets, and $q_\gamma = |\boldsymbol{q}_\gamma| = E_\gamma$, $q_\pi = |\boldsymbol{q}_\pi|$ and $q_{f,s} = |\boldsymbol{q}_{f,s}|$; m_d, m_π, m_p, m_n are the deuteron, pion, proton, and neutron masses. In the unpolarized case one can rewrite Eq. (10) with the full set of variables as

$$\frac{d\sigma_{\gamma p}}{d\Omega}(W, z; m_p'^2) = \frac{1}{n(\boldsymbol{q}_s)} \frac{d\sigma_{\gamma d}}{d\Omega\, d\boldsymbol{q}_s}(E_\gamma, z, \varphi, q_s, z_s), \quad n(\boldsymbol{q}_s) = \frac{E'_\gamma}{E_\gamma}\rho(q_s). \qquad \text{(A.2)}$$

In Eq. (A.2) is $d\Omega = dz d\varphi$ ($z = \cos\theta$) the solid angle element of outgoing the π^0 in the $\pi^0 p$ center-of-mass frame with the z-axis along the photon beam, where θ and φ are the corresponding polar and azimuthal angles. The laboratory polar angle of the neutron spectator is θ_s with $z_s = \cos\theta_s$. W is the effective $\pi^0 p$ mass related to $\boldsymbol{q}_s$ by

$$W^2 = (k_\gamma + p_d - p_s)^2 = (E_\gamma + m_d - E_s)^2 - E_\gamma^2 - q_s^2 + 2E_\gamma q_s z_s \quad (E_s = \sqrt{m_n^2 + q_s^2}) \qquad \text{(A.3)}$$

The momentum-distribution function $\rho(q)$ and photon laboratory energy E'_γ in the subprocess $\gamma p \to \pi^0 p$ are defined in connection with Eq. (10). One can also write $E'_\gamma = (W^2 - m_p^2)/2m_p$.

For a given E_γ, the cross section $d\sigma_{\gamma d}/d\Omega\, d\boldsymbol{q}_s$ with unpolarized particles depends in general case on four variables, chosen in Eq. (A.2) as z, φ, q_s and z_s. The cross section $d\sigma_{\gamma p}/d\Omega$, being a function of W and z, may also depend on the virtuality $m_p'^2$ of the "target" proton in the subrocess $\gamma p \to \pi^0 p$, where $m_p'^2 = (p_d - p_s)^2 = (m_d - E_s)^2 - q_s^2 \neq m_p^2$. Thus, in view of Eq. (A.3) the cross section $d\sigma_{\gamma p}/d\Omega$ in Eq. (A.2) depends only on three variables, i.e., q_z, z_s and z. Thus, the cross section $d\sigma_{\gamma d}/d\Omega\, d\boldsymbol{q}_s$ on the deuteron should not depend on φ in the model based on the leading IA diagram M_{a1} in Fig. 1.

For completeness, let us express the cosine z in Eq. (A.2) through the particle momenta from Eq. (A.1). It can be obtained through the relations

$$(k_\gamma k_\pi) = E_\gamma^c (E_\pi^c - q_\pi^c z), \quad E_\gamma^c = \frac{W^2 - m_p'^2}{2W}, \quad E_\pi^c = \frac{W^2 + m_\pi^2 - m_p^2}{2W}, \quad q_\pi^c = \sqrt{(E_\pi^c)^2 - m_\pi^2}, \quad \text{(A.4)}$$

where E_γ^c and E_π^c are the total energies of the photon and pion in the $\pi^0 p$ center-of-mass frame.

Let us rewrite Eq. (A.2) in a form more convenient for applications. Making the substitutions $d\Omega = dzd\varphi$ and $d\boldsymbol{q}_s = q_s^2 dq_s dz_s d\varphi_s$ and averaging Eq. (A.2) over φ and φ_s, we obtain

$$\frac{d\sigma_{\gamma p}}{dz}(W, z; m_p'^2) = \frac{1}{2\pi n(\boldsymbol{q}_s)} \frac{d^3\sigma_{\gamma d}}{q_s^2 dq_s\, dz dz_s}(E_\gamma, z, q_z, z_s). \tag{A.5}$$

In the real data analysis, one may divide the phase space of the reaction $\gamma d \to \pi^0 pn$ into small cubes, bounded by the values

$$z \pm \frac{1}{2}\Delta_z, \qquad q_s \pm \frac{1}{2}\Delta_{q_s}, \qquad z_s \pm \frac{1}{2}\Delta_{z_s}. \tag{A.6}$$

Let $\Delta\sigma(E_\gamma, z, q_s, z_s)$ be the $\gamma d \to \pi^0 pn$ cross section in such a cube (A.6). Then, we get

$$\frac{d\sigma_{\gamma p}}{dz}(W, z; m_p'^2) = \frac{1}{2\pi n(\boldsymbol{q}_s)} \frac{\Delta\sigma(E_\gamma, z, q_s, z_s)}{\Delta_z \Delta_{z_s} \Delta_{q_s} q_s^2}, \qquad n(\boldsymbol{q}_s) = \frac{E'_\gamma}{E_\gamma}\rho(q_s), \tag{A.7}$$

where $W^2 = W^2(E_\gamma, q_s, z_s) =$ Eq. (A.3), $E'_\gamma = (W^2 - m_p^2)/2m_p$, and $m_p'^2 = (m_d - E_s)^2 - q_s^2$. At small q_s ($\ll m_{p,n}$), one may neglect the q_s^2 terms in $m_p'^2$ and W^2 (A.3). Then $m'_p = m_p$, but W depends on q_s and z_s through the linear term $2E_\gamma q_s z_s$ in Eq. (A.3), and $E'_\gamma = E_\gamma[1 + (q_s/E_s)z_s]$.

References

[1] G. Chew and M. Goldberger, Phys. Rev. **87**, 778 (1952).

[2] F. A. Berends, A. Donnachie, and D. L. Weaver Nucl. Phys. B **4**, 1 (1967).

[3] V. E. Tarasov, W. J. Briscoe, H. Gao, A. E. Kudryavtsev, and I. I. Strakovsky, Phys. Rev. C **84**, 035203 (2011). The results of this paper was applyed for analysis of the $\gamma d \to \pi^- pp$ data in the papers: W. Chen, H. Gao, W. J. Briscoe, D. Dutta, A. E. Kudryavtsev, M. Mirazita, M.W. Paris, P. Rossi, S. Stepanyan, I. I. Strakovsky, V. E. Tarasov, and R. L. Workman, Phys. Rev. C **86**, 015206 (2012); W. J. Briscoe, A. E. Kudryavtsev, P. Pedroni, I. I. Strakovsky, V. E. Tarasov, and R. L. Workman, Phys. Rev. C **86**, 065207 (2012).

[4] A. Fix and H. Arenhovel, Phys. Rev. C **72**, 064004 (2005); 064005 (2005).

[5] M. I. Levchuk, A. Yu. Loginov, A. A. Sidorov, V. N. Stibunov, and M. Schumacher, Phys. Rev. C **74**, 014004 (2006).

[6] E. M. Darwish, Ph.D. thesis, University of Mainz, 2003.

[7] A. B. Migdal, JETP **1**, 2 (1955); K. M. Watson, Phys. Rev. **88**, 1163 (1952).

[8] I. Blomqvist and J.-M. Laget, Nucl. Phys. **A280**, 405 (1977).

[9] W. J. Briscoe, I. I. Strakovsky, and R. L. Workman, Institute of Nuclear Studies of The George Washington University Database; http://gwdac.phys.gwu.edu/analysis/pr_analysis.html. For our calculations, we used recent SAID CM12 solution, R. L. Workman, M. W. Paris, W. J. Briscoe, and I. I. Strakovsky, Phys. Rev. C **86**, 015202 (2012).

[10] R. A. Arndt, W. J. Briscoe, I. I. Strakovsky, and R. L. Workman, Phys. Rev. C **66**, 055213 (2002); M. Dugger, J. P. Ball, P. Collins, E. Pasyuk, B. G. Ritchie, R. A. Arndt, W. J. Briscoe, I. I. Strakovsky, R. L. Workman *et al.* (CLAS Collaboration), Phys. Rev. C **76**, 025211 (2007).

[11] L. D. Landau and E. M. Livshits, *Quantum Mechanics: Non-Relativistic Theory*, Vol. 3, (Pergamon Press, 1977).

[12] R. A. Arndt, W. J. Briscoe, I. I. Strakovsky, and R. L. Workman, Phys. Rev. C **74**, 045205 (2006).

[13] R. Machleidt, K. Holinde, and C. Elster, Phys. Rep. **149**, 1 (1987).

[14] D. Werthmüller *et al.*, Phys. Rev. Lett. **111**, 232001 (2013).

[15] D. Werthmüller *et al.*, Phys. Rev. C **90**, 015205 (2014).

[16] A. Fix, H. Arenhovel, M. Levchuk, and M. Tammam, Phys. Rev. C **91**, 014001 (2015).

[17] B. Krusche, J. Ahrens, R. Beck, M. Fuchs, S. J. Hall, F. Härter, J. D. Kellie, V. Metag, M. Röbig-Landau, and H. Ströher, Eur. Phys. J. A **6**, 309 (1999).

[18] M. Dieterle *et al.*, Phys. Rev. Lett. **112**, 142001 (2014).

[19] V. M. Kolybasov and V. G. Ksenzov, JETP **44**, 6 (1976) [ZhETF **71**, 13 (1976)].

[20] G. A. Miller, B. M. K. Nefkens, and I. Šlaus, Phys. Rep. **194**, 1 (1990).